



Generation of Field-Aligned Currents in Response to Sudden Enhancement of Solar Wind Dynamic Pressure

Tian Zhang¹ , Yusuke Ebihara¹ , and Takashi Tanaka² 

¹Research Institute for Sustainable Humanosphere, Kyoto University, Uji, Japan, ²International Center for Space and Planetary Environmental Science, Kyushu University, Fukuoka, Japan

Key Points:

- The origin of field-aligned currents (FACs) associated with solar wind dynamic pressure pulse is identified by tracing a packet of Alfvén waves in MHD simulation
- PI FACs are generated off equator at leading edge of compressional wave and MI FACs are generated in equatorial plane behind leading edge
- The polarity of PI FAC is determined by vorticity, while that of MI FAC is determined by the dot product of current density and velocity

Correspondence to:

T. Zhang and Y. Ebihara,
zhang.tian.74r@st.kyoto-u.ac.jp;
zt136515@gmail.com;
ebihara@rish.kyoto-u.ac.jp

Citation:

Zhang, T., Ebihara, Y., & Tanaka, T. (2024). Generation of field-aligned currents in response to sudden enhancement of solar wind dynamic pressure. *Journal of Geophysical Research: Space Physics*, 129, e2024JA032768. <https://doi.org/10.1029/2024JA032768>

Received 19 APR 2024

Accepted 11 SEP 2024

Abstract We investigated the generation of field-aligned currents (FACs) in response to the sudden enhancement of the solar wind dynamic pressure by tracing backward in time a packet of the Alfvén wave in the global magnetohydrodynamic (MHD) simulation. The generation region is identified from three perspectives, including the continuity of the current, the energy conservation and the time rate of change in the FACs. The generation mechanism is found to be related with the tailward motion of the compressional wave, which is excited when the magnetopause is compressed due to the solar wind dynamic pressure pulse. The compressional wave with a high magnetic pressure center interacts with the Earth's dipole field and forms a protruding part of the wavefront near the equatorial plane. The leading edge of the merged magnetic pressure that pertains to the compressional wave and the Earth starts to generate preliminary impulse (PI) FACs off the equator, as the magnetic pressure force accelerates the plasma and magnetic field lines are bent (FAC dynamo 1). Main impulse (MI) FACs are generated behind the leading edge in the equatorial plane due to the enhanced magnetic tension force (FAC dynamo 2). Magnetic field lines would be extremely curved during the passage due to the increasing magnetic tension force. The polarity of PI FACs is decided by the parallel vorticity of plasma flow, and MI FACs are the result of enhanced perpendicular currents together with the plasma flow in the equatorial plane.

Plain Language Summary Sudden commencement (SC) is an impulse response of the magnetosphere-ionosphere system caused by an abrupt change in the dynamic pressure of solar wind. However, the generation of SC-associated field-aligned currents (FACs) is not well understood. The magnetohydrodynamic (MHD) simulations are employed to investigate the FACs in response to the solar wind dynamic pressure pulse. A new method of tracing Alfvén wave packets is used to identify the generation region and mechanism of the FACs associated with the SCs in the simulation. The results show that the generation of preliminary impulse (PI) FACs is off the equator and related with the acceleration by magnetic pressure force; main impulse (MI) FACs are associated with the deceleration of plasma flow in the equatorial plane by magnetic tension force. The polarity of PI and MI FACs depends on two different mechanisms.

1. Introduction

Sudden commencement (SC) is the so-called ground manifestation of two abrupt and successive geomagnetic disturbances, namely the preliminary impulse (PI) and the main impulse (MI), in response to the jump in solar wind dynamic pressure (e.g., Araki, 1994; Araki & Allen, 1982; Fujita & Tanaka, 2022; Fujita, Tanaka, Kikuchi, Fujimoto, Hosokawa, & Itonaga, 2003; Fujita, Tanaka, Kikuchi, Fujimoto, & Itonaga, 2003; Fujita et al., 2005; Kikuchi et al., 2016, 2022; Tamao, 1964). It usually exhibits a step-function like increase in the H -component (the horizontal component of the disturbance geomagnetic field) at mid- and low-latitudes (DL), and bipolar variations at auroral latitudes (DP). The study of SCs from the global magnetic observations has a long history since the great progress made during the IGY 1957–58 (e.g., Akasofu & Chapman, 1959; Matsushita, 1957; Wilson & Sugiura, 1961).

These observed facts mentioned above are explained by assuming that the ionospheric electric field associated with a pair of upward and downward field-aligned currents (FACs) induces such ground magnetic disturbances through the Hall currents (Araki, 1994). It has been found that the ionospheric Hall current associated with the PI shows a double-cell structure (anticlockwise vortex in the dawn hemisphere, and clockwise vortex in the dusk hemisphere) at high latitudes, followed by a subsequent MI-associated vortex with an opposite sense of the Hall current flowing (e.g., Moretto et al., 2000). The generation mechanism of FACs plays an important role in understanding this very transient physical process.

© 2024 The Author(s).

This is an open access article under the terms of the [Creative Commons Attribution-NonCommercial License](https://creativecommons.org/licenses/by/4.0/), which permits use, distribution and reproduction in any medium, provided the original work is properly cited and is not used for commercial purposes.

Many studies based on both observational data analysis and numerical simulation have been done. Tamao (1964) theoretically interpreted the cause of the PI-associated current as the mode conversion from fast magnetosonic wave generated by sudden compression of the dayside magnetosphere to the Alfvén wave. It is suggested that the mode conversion takes place where the spatial gradient of the Alfvén speed arises. Fujita, Tanaka, Kikuchi, Fujimoto, Hosokawa, and Itonaga (2003) and Fujita, Tanaka, Kikuchi, Fujimoto, and Itonaga (2003) showed that the excitation of the FAC coincides with the region where the gradient of the Alfvén wave is large, and suggested that the mode conversion from the fast magnetosonic wave to the Alfvén wave occurs. The mode conversion region is clarified to be in the outer magnetosphere through tracing a current line by Fujita and Tanaka (2022), which remains to be verified by observation. An induced dusk-to-dawn electric field following the sudden compression is considered as the source that gives rise to the FACs during PI phase in some other studies (e.g., Araki, 1994; Moretto et al., 2000; Yu et al., 2022; Yu & Ridley, 2009). For MI FACs, many studies (e.g., Araki, 1994; Fujita & Tanaka, 2006; Guo & Hu, 2007; Tian et al., 2016; Yu & Ridley, 2009) suggested that the generation is related with a plasma vortex just after the passage of the compressional wave, and the vortex is more dominant during the late stage of MI phase. This process may repeat (e.g., Fujita et al., 2012), since wave-like oscillations are observed in the geomagnetic data as reported in (Hori et al., 2012; Yu & Ridley, 2011).

The current generator (dynamo) region is determined by condition $\mathbf{J} \cdot \mathbf{E} < 0$ (where \mathbf{J} and \mathbf{E} are the current density and the electric field, respectively), which is widely used (e.g., Siscoe et al., 2000; Tanaka, 1995). The negative value stands for energy transfer from plasma flow to electromagnetic energy. Samsonov et al. (2010) investigated the intensification of northward B_z (NBZ) and Region 1 currents (near the poleward edge of the auroral zone, downward on the dawnside and upward on the duskside, Iijima & Potemra, 1976; Zmuda & Armstrong, 1974) due to the interplanetary shock, and identified two strong dynamo regions in the magnetosphere based on this condition. However, Ebihara and Tanaka (2022) pointed out that this criterion ($\mathbf{J} \cdot \mathbf{E} < 0$) does not always mean the generation of Alfvén waves when magnetic pressure force is nonnegligible (see detailed explanation in Section 4).

Keller et al. (2002) found that the generation locations for both PI and MI FACs were in the magnetosphere in response to a density jump of solar wind by mapping FACs along the magnetic field lines. Tracing a magnetic field line from the ionosphere is the most popular method when investigating the generation region of FACs, while FACs do not always flow just along magnetic field lines. Another method of tracing current lines is used by Fujita and Tanaka (2022), who claimed that there were two current systems in PI phase of SCs. Sun et al. (2014) linked the MI-associated geomagnetic response with the negative magnetic field disturbance (magnetic field decreases due to interplanetary shocks) in nightside magnetosphere by tracing the current lines. Whereas the location of current lines would be affected by the field-perpendicular current and do not always pass through the generation region of FACs in the simulations (Ebihara & Tanaka, 2024). This method of tracing current lines may not be able to identify the generation region precisely either.

Thus, we followed a new approach proposed by Ebihara and Tanaka (2022, 2023), who identified the generation region of Region-1 FACs and substorm-associated FACs by tracing a packet of Alfvén wave. The FAC dynamo region is defined therein from the following three aspects based on fundamental physics. The first perspective is the continuity of the current. When FACs are generated, the divergence of the FACs should not be zero due the conservation law. The second one is the time rate of change in the FACs, which should be nonzero, indicating the current is generating. The last is the negative work against the magnetic tension force performed by the plasma, which is supposed to excite the Alfvén waves (see details in Section 2.3).

The aim of this study is to understand the generation of FACs in response to the solar wind pressure pulse. The key issues to be settled include where and how the FACs are generated, the reason why there are bidirectional FACs on the same side (dawn or dusk), considering if they are generated by the same mechanism, and what causes the change in the polarity of the FACs during different impulse phases. Thus, the new method that traces the Alfvén wave packet is employed, which enables us to identify the generation region of FACs precisely combined with three criteria mentioned above and obtain the quantities required in the analysis of the simulation result that may help to make clear the generation process. The results are explained in terms of dynamo regions, corresponding to the physical processes in the passage of the compressional wave excited by the impact of solar wind dynamic pressure on the dayside magnetosphere.

2. Method

2.1. Global MHD Simulation

The global MHD simulation code “Reproduce Plasma Universe (REPPU)” is developed by T. Tanaka and the details are explained in his papers (Tanaka, 1994, 1995, 2015). The coordinate system in the magnetospheric domain is set as that the origin is at the center of the Earth, the x -axis points sunward, the z -axis points to the north, and the y -axis is chosen to satisfy the right-handed system correspondingly. The outer boundary conditions correspond to the solar wind on the upstream side at $x = 600 R_E$ at noon and a zero gradient on the downstream side at $x = 200 R_E$ at midnight. The inner boundary is at $2.6 R_E$. The grid system is constructed by a sixth-order triangulation with 320 radially stacked spheres. The MHD domain with 30,722 grids is coupled with the ionospheric domain (Ebihara et al., 2014). The grid spacing in the outward direction is $0.044 R_E$ at the inner boundary, and $0.22 R_E$ at $12 R_E$ at midnight in the equatorial plane (Ebihara & Tanaka, 2015). This coupling process considers four aspects: (a) the mapping of instantaneous values of FACs, plasma pressure and temperature from the inner boundary to the ionosphere; (b) the calculation of the height-integrated ionospheric conductivity that is decided by the solar extreme ultraviolet (EUV), and both the contribution from precipitation associated with discrete aurorae and diffuse aurorae; (c) the requirement of current continuity; and (d) the mapping of electric field from the ionosphere to the inner boundary along the dipole magnetic field line (Ebihara & Tanaka, 2022).

The simulation is started from a quasi-stationary state with solar wind parameters of $N_{sw} = 5/cc$, $V_{sw} = 400$ km/s, $B_y = 0$ nT, $B_z = 3$ nT, where N_{sw} is the solar wind density and V_{sw} is the solar wind velocity. The pressure pulse was imposed by increasing V_{sw} from 400 to 1,000 km/s, and N_{sw} from 5/cc to 50/cc at $x = 40 R_E$. The solar wind condition is changed at $T = 120$ min (elapsed time of simulation). The IMF B_z remains northward. The tracing method described in detail below to identify the generation region of the FACs is proposed by Ebihara and Tanaka (2022, 2023).

2.2. Alfvén Wave Packet Tracing

It is assumed that the perturbation associated with the FACs propagates at the characteristic velocity \mathbf{v} (Neubauer, 1980; Wright & Southwood, 1987) as

$$\begin{aligned} \mathbf{v} &= \pm \mathbf{V}_A + \mathbf{V}, \\ \mathbf{V}_A &= \mathbf{B} / \sqrt{(\mu_0 \rho)}, \end{aligned} \quad (1)$$

where \mathbf{V}_A is the Alfvén velocity, \mathbf{V} is the flow velocity of plasma, ρ is the mass density of plasma and μ_0 is the magnetic constant. The group velocity of the Alfvén wave moves along the background magnetic field in the rest frame of the moving medium (Walker, 2008). The sign \pm indicates the motion is parallel (+) or antiparallel (−) to the magnetic field, separately. The packet of Alfvén wave carrying the information associated with the FACs could be located by the equation below (Ebihara & Tanaka, 2022, 2023):

$$\mathbf{r}(t) = \int_0^t \mathbf{v}(\mathbf{r}, \tau) d\tau + \mathbf{r}_0, \quad (2)$$

where \mathbf{r}_0 is the starting point of tracing. The inner boundary of the MHD domain is located at $2.6 R_E$. The packets were first traced from the ionosphere to a sphere at a radius of $3.9 R_E$ along the dipole magnetic field line, then from this sphere to the further region using Equations 1 and 2 with positive \mathbf{V}_A (Ebihara & Tanaka, 2023).

2.3. Identification of FAC Generation

Three criteria of FAC dynamo mentioned in the introduction are described as follows.

1. The first criterion is based on the current continuity,

$$\begin{aligned} \nabla \cdot \mathbf{J}_{\parallel} + \nabla \cdot \mathbf{J}_{\perp} &= 0, \\ \mathbf{J}_{\perp} &= \mathbf{J}_d + \mathbf{J}_i \end{aligned} \quad (3)$$

where $\nabla \cdot \mathbf{J}_{\parallel} \neq 0$, indicating the field-perpendicular current (including the diamagnetic current \mathbf{J}_d and the inertial current \mathbf{J}_i) is converted to the FAC.

2. The second criterion is the nonzero rate of change in the FAC (Itonaga et al., 2000; Song & Lysak, 2001),

$$\begin{aligned} \frac{\partial J_{\parallel}}{\partial t} &= -\frac{1}{\mu_0} (\nabla \times \nabla \times \mathbf{E})_{\parallel} \\ &= \frac{-\nabla_{\parallel} (\nabla \cdot \mathbf{E})}{\mu_0} + \frac{(\nabla^2 \mathbf{E})_{\parallel}}{\mu_0}, \end{aligned} \quad (4)$$

where \mathbf{E} is the electric field and only \mathbf{E}_{\perp} is present under the ideal MHD approximation. The displacement current is omitted.

3. The third criterion is associated with the excitation of Alfvén waves. To understand the origin of Alfvén waves, it is relevant to define the magnetic tension first. The Lorentz force is

$$\begin{aligned} \mathbf{F} &= \mathbf{J} \times \mathbf{B} \\ &= \frac{1}{\mu_0} (\nabla \times \mathbf{B} \times \mathbf{B}), \end{aligned} \quad (5)$$

with the vectorial identity, we obtain

$$\begin{aligned} \mathbf{F} &= \frac{1}{\mu_0} (\nabla \times \mathbf{B} \times \mathbf{B}) \\ &= -\nabla \left(\frac{B^2}{2\mu_0} \right) + (\mathbf{B} \cdot \nabla) \frac{\mathbf{B}}{\mu_0}, \end{aligned} \quad (6)$$

where the Lorentz force involves two terms. The generation of an Alfvén wave could be described as the magnetic field line is first bent due to the motion together with the plasma according to frozen-in theorem, and then magnetic tension appears in the field line, so the plasma performs negative work against the tension force. Based on Ebihara and Tanaka (2022, 2023), the Lorentz force \mathbf{F} is decomposed into the magnetic pressure force \mathbf{F}_m and the magnetic tension force \mathbf{F}_t as

$$\begin{aligned} \mathbf{F} &= \mathbf{F}_m + \mathbf{F}_t, \\ \mathbf{F}_m &\equiv -\nabla_{\perp} \left(\frac{B^2}{2\mu_0} \right), \\ \mathbf{F}_t &\equiv (\mathbf{B} \cdot \nabla) \frac{\mathbf{B}}{\mu_0} - \nabla_{\parallel} \left(\frac{B^2}{2\mu_0} \right) \\ &= \frac{B^2}{\mu_0} (\mathbf{b} \cdot \nabla) \mathbf{b}, \end{aligned} \quad (7)$$

where \mathbf{b} is the unit vector of the magnetic field ($=\mathbf{B}/B$), and $B^2/2\mu_0$ is the magnetic pressure. Ebihara and Tanaka (2022) pointed out that $(\mathbf{J} \cdot \mathbf{E} = \mathbf{V} \cdot \mathbf{F} < 0)$ is not necessarily associated with the generation of Alfvén waves when the magnetic pressure force is present. Thus, the last criterion is given as

$$\mathbf{V} \cdot \mathbf{F}_t < 0. \quad (8)$$

Magnetic tension is necessary for exciting Alfvén waves. Although this condition indicates the excitation of Alfvén waves, it does not always generate FACs (Cravens, 1997; Ebihara & Tanaka, 2024). Consequently, all the three criteria listed above must be satisfied when identifying the generation of FACs. For example, for a downward FAC ($J_{\parallel} > 0$) transported by an Alfvén wave parallel to the magnetic field ($V_A > 0$) in the Northern

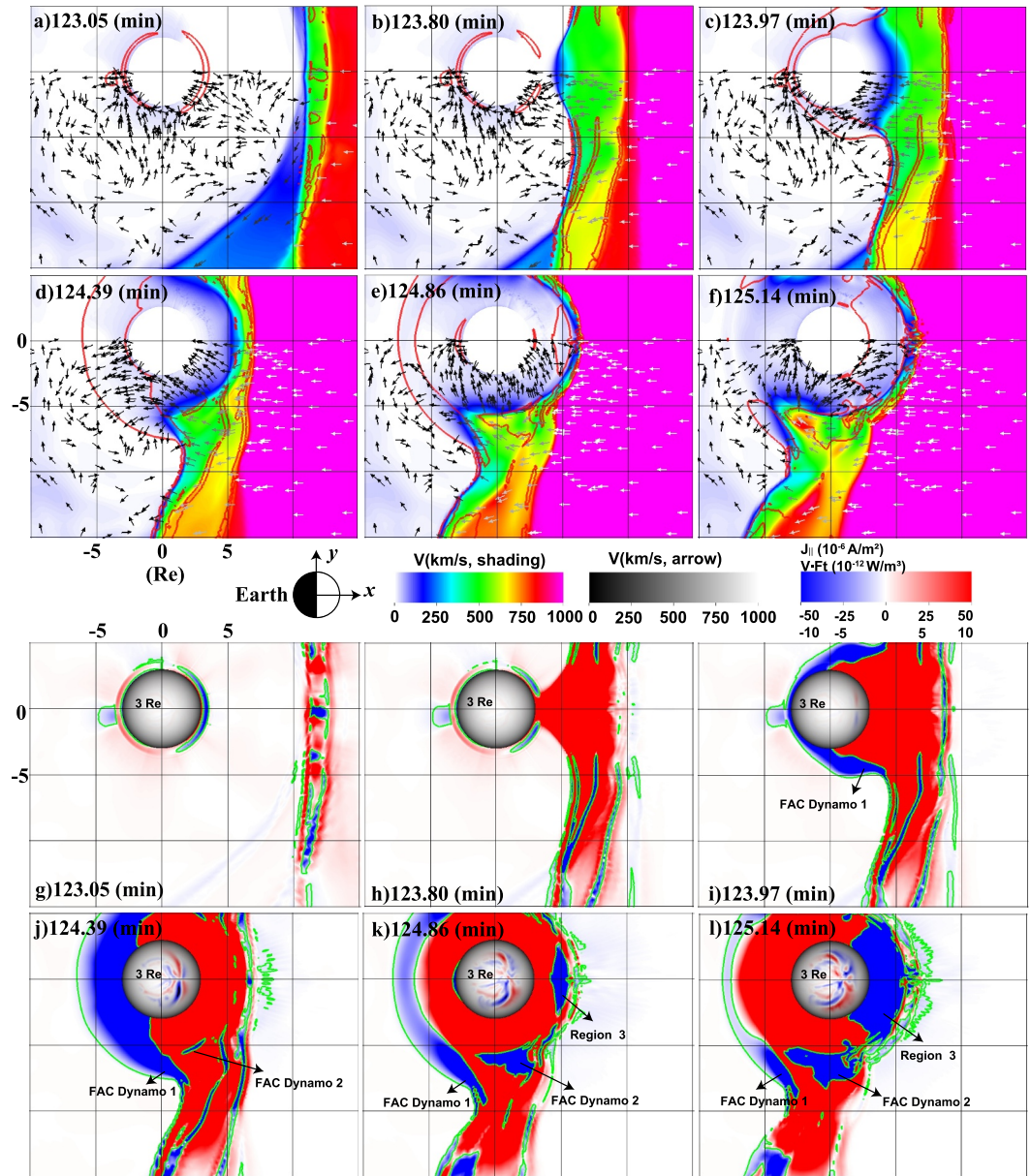


Figure 1. A time sequence of six snapshots of the MHD simulation in the equatorial plane ($z = 0$). Sun is to the right. Top 6 panels (from a to f) show the evolution of plasma flow velocity; blank area marks the inner boundary; colors and arrows indicate the magnitude and direction of the plasma flow. Bottom 6 panels (from g to l) indicate the evolution of FACs on $3 R_E$ sphere and $\mathbf{V} \cdot \mathbf{F}_t$ in the equatorial plane; magnitude and polarity of FACs and $\mathbf{V} \cdot \mathbf{F}_t$ are indicated by colored shadings, red for positive and blue for negative.

Hemisphere, the three conditions based on the above criteria should be as follows: $\nabla \cdot \mathbf{J}_{||} > 0$, $\partial J_{||} / \partial t > 0$, and $\mathbf{V} \cdot \mathbf{F}_t < 0$.

3. Results

3.1. Candidate Dynamo Regions (Where $\mathbf{V} \cdot \mathbf{F}_t < 0$) in the Magnetosphere

Figure 1 shows the evolution of the velocity of plasma flow (Figures 1a–1f) and the distribution of $\mathbf{V} \cdot \mathbf{F}_t$ (Figures 1g–1l) in the equatorial plane after the propagation of the sudden pressure pulse according to the MHD simulations. The discussion in this paper is focused only on the dawnside due to IMF $B_y = 0$. The red curves in top

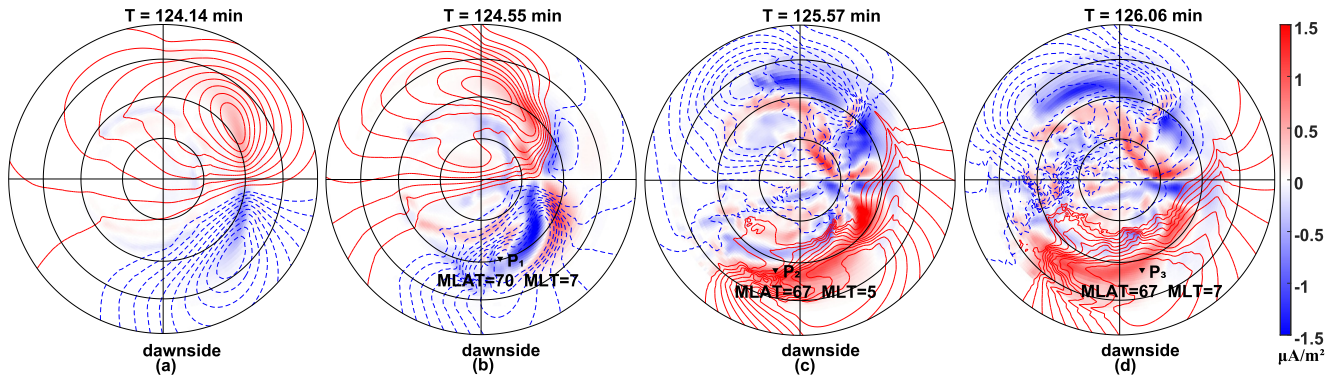


Figure 2. Snapshots of the footprints of the FACs and the electric potential in the ionosphere. Negative/positive values indicate upward/downward FACs (bluish/reddish). Sun is to the right, and the outermost circle represents the magnetic latitude of 50° . The solid/dashed contour lines represent positive/negative potential, respectively. The triangles in black indicate the starting point of tracing from the ionosphere.

6 panels (from a to f) correspond to $\mathbf{V} \cdot \mathbf{F}_t = -2.0 \times 10^{-12} \text{ W/m}^3$, and the green curves in bottom 6 panels (from g to l) correspond to $\mathbf{V} \cdot \mathbf{F}_t = -1.0 \times 10^{-12} \text{ W/m}^3$. These red and green lines are surrounding the Earth at the early stage due to the Earth's intrinsic magnetic field. The change in the colors of shadings in Figures 1a–1f indicates the location of bow shock and magnetopause as the solar wind is suddenly decelerated there. Figure 1a shows that the impulse front encounters the magnetopause at around $T = 123.05 \text{ min}$, the magnetopause starts to move inward and this results in a compressional wave propagating into the magnetosphere (Samsonov & Sibeck, 2013). The compressional front is in a convex shape, and shortly deformed by the touch of a particular boundary as shown in Figure 1b. The front part across the Sun-Earth line becomes a concave shape (Samsonov et al., 2007), and extends forward through the flank continuously toward nightside according to Figure 1c. When the PI FACs start to appear in the $3 R_E$ sphere as shown in Figure 1i, the first $\mathbf{V} \cdot \mathbf{F}_t < 0$ region located at the compressional front is developing. We call it FAC dynamo 1. Soon later, the plasma behind the compressional front flows along the boundary, and then another region with $\mathbf{V} \cdot \mathbf{F}_t < 0$ is formed on the dayside in Figures 1d and 1j. We call it FAC dynamo 2. Meanwhile, the plasma is decelerated and diverted near the dawnside. Later, on the dayside the plasma inside the boundary moves sunward instead, and another region near noon with $\mathbf{V} \cdot \mathbf{F}_t < 0$ appears as shown in Figures 1e and 1k. This region is called Region 3, expanding rapidly toward nightside. The slow sunward plasma flow inside the boundary together with the outside fast anti-sunward flow develops into a flow vortex (Fujita, Tanaka, Kikuchi, Fujimoto, & Itonaga, 2003; Samsonov & Sibeck, 2013; Shi et al., 2014; Sibeck, 1990) according to Figure 1f. It should be noted that the naming of the three regions is based on that FACs are generated in the first two regions, so they are called FAC dynamo 1 and 2 (to distinguish with the existed Region-1 and Region-2 FACs), but no FACs are generated in Region 3 according to the following study. Both of FAC dynamo 1 and 2 have a 3-D structure.

3.2. Footprints of the FACs in the Ionosphere

Figure 2 shows the FACs (color shadings) and the electric potential (contour lines) in the ionosphere taken at $T = 124.55$, 125.57 and 126.06 min . The solar wind velocity is increased from 400 to $1,000 \text{ km/s}$ and the solar wind density is increased from $5/\text{cc}$ to $50/\text{cc}$. The whole evolution of the simulated SC in response to the pressure pulse could be found in Zhang et al. (2023a, 2023b). A pair of FACs corresponding to PI (upward on the dawnside, and downward on the duskside) appear first in Figure 2a. Then, the other pair of FACs with the opposite sense corresponding to MI appear and move in the anti-sunward direction. Figure 2b shows a snapshot at $T = 124.55 \text{ min}$ when PI and MI FACs had appeared in the ionosphere. We chose a point that is located at the leading edge of PI-associated upward FAC on the dawnside, and call it P_1 . Figure 2c is taken at $T = 125.57 \text{ min}$ when MI keeps developing and moving anti-sunward. We chose a point that is located at the leading edge of MI-associated downward FAC on the dawnside. We call this point P_2 . Figure 2d shows the snapshot at $T = 126.06 \text{ min}$, corresponding to a very late stage of SC. We chose a point in the heart of the MI-associated downward FAC, and call it point P_3 . The corresponding tracing of the Alfvén wave packets associated with the three moments is started from the point P , located at the ionospheric altitude, then along the magnetic field line to the point Q (see details in Table 1) on the sphere with a radius of $3.9 R_E$ (to avoid uncertainty in the calculation

Table 1
Locations on the Trajectory of Traced Alfvén Wave Packets

MHD time T (min)	Point on the ionosphere P (MLT, MLAT)	Point on $3.9 R_E$ Q (x, y, z) ^a
124.55	P_1 (7, 70)	Q_1 (0.63, -2.59, 2.84)
125.57	P_2 (5, 67)	Q_2 (-1.04, -3.02, 2.28)
126.06	P_3 (7, 67)	Q_3 (0.71, -3.11, 2.38)

^a x, y, z in unit of R_E .

of the Alfvén velocity near the inner boundary). The tracing would continue from this sphere backward in time in the way as expressed in Equations 1 and 2. The trajectories of the packets from P_1, P_2 and P_3 shown in Figures 3–5 are connecting to three $\mathbf{V} \cdot \mathbf{F}_t < 0$ regions in Figure 1, separately. In fact, most points distributed in the footprints as shown in Figure 2 were selected as the start point of tracing to find the generation region, but only those in a small region satisfied three criteria. We chose the points (P_1 and P_2) in this region, because the generation of the FACs is clearly identified near the leading edges of the PI- and MI-associated FAC regions.

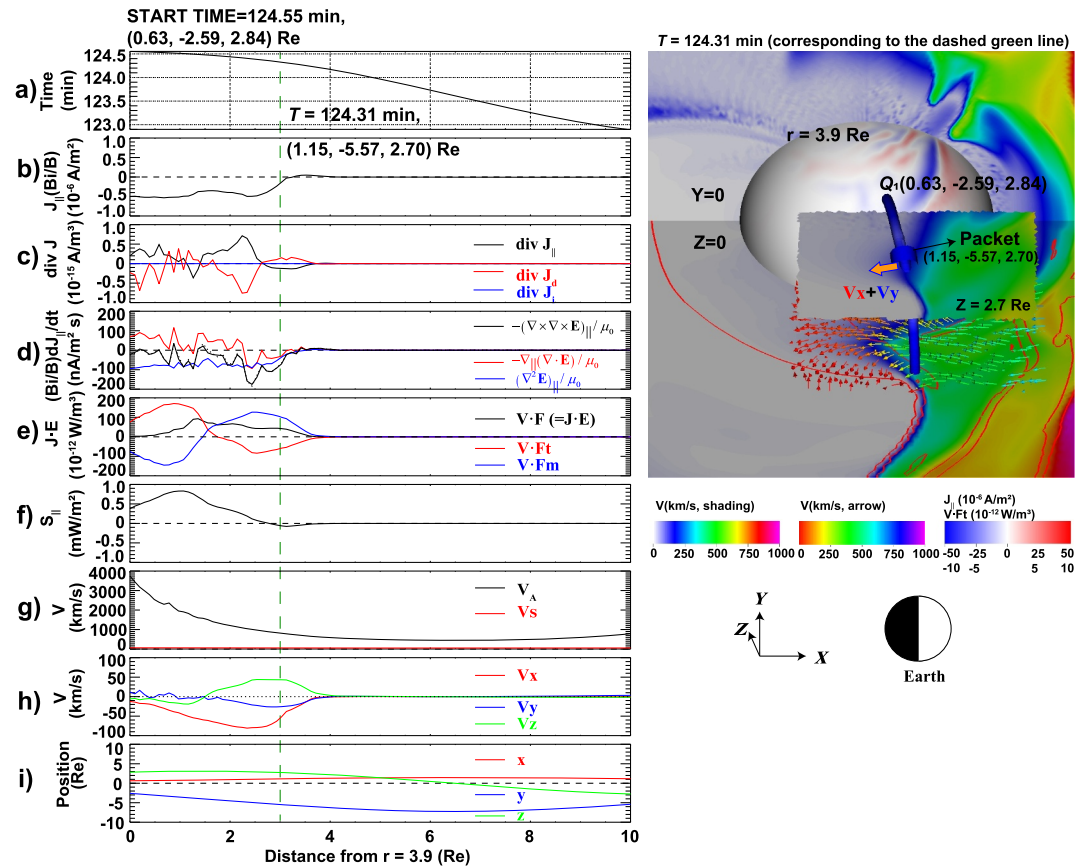


Figure 3. Quantities taken along the trajectory of the packet of the Alfvén wave associated with PI. The horizontal axis marks the distance from $r = 3.9 R_E$, and vertically aligned panels in the left column are (a) elapsed time, (b) normalized field-aligned current (FAC) $(B_{\parallel}/B) J_{\parallel}$ (positive parallel and negative anti-parallel to the magnetic field), (c) $\nabla \cdot \mathbf{J}_{\parallel}$, $\nabla \cdot \mathbf{J}_d$, and $\nabla \cdot \mathbf{J}_i$, where \mathbf{J}_{\parallel} , \mathbf{J}_d and \mathbf{J}_i are the FAC, the diamagnetic current and the inertial current, respectively, (d) the rate of change in the FAC, $\partial J_{\parallel} / \partial t$, consists of $-\nabla_{\parallel}(\nabla \cdot \mathbf{E}) / \mu_0$ (red line) and $(\nabla^2 \mathbf{E})_{\parallel} / \mu_0$ (blue line), (e) $\mathbf{J} \cdot \mathbf{E}$ (black), $\mathbf{V} \cdot \mathbf{F}_t$ (red) and $\mathbf{V} \cdot \mathbf{F}_m$ (blue), where \mathbf{F}_t and \mathbf{F}_m are the magnetic tension force and the magnetic pressure force, respectively, (f) parallel Poynting flux S_{\parallel} , (g) velocity of Alfvén speed and sound speed, (h) velocity of plasma, and (i) the position of the packet. In the right column, a snapshot taken at $T = 124.31$ min is displayed, showing the location of the Alfvén wave packet on the trajectory from the equatorial plane to Q_1 on the $3.9 R_E$ sphere (color of shadings on the sphere indicates intensity of FACs). The magnitude of the plasma velocity is shown in the x - y and x - z planes. Arrows in the x - y plane at $z = 0$ and $z = 2.7 R_E$ indicate the magnitude and direction of flow velocity. The color of tubes and shadings indicate the value of $\mathbf{V} \cdot \mathbf{F}_t$ and J_{\parallel} , separately.

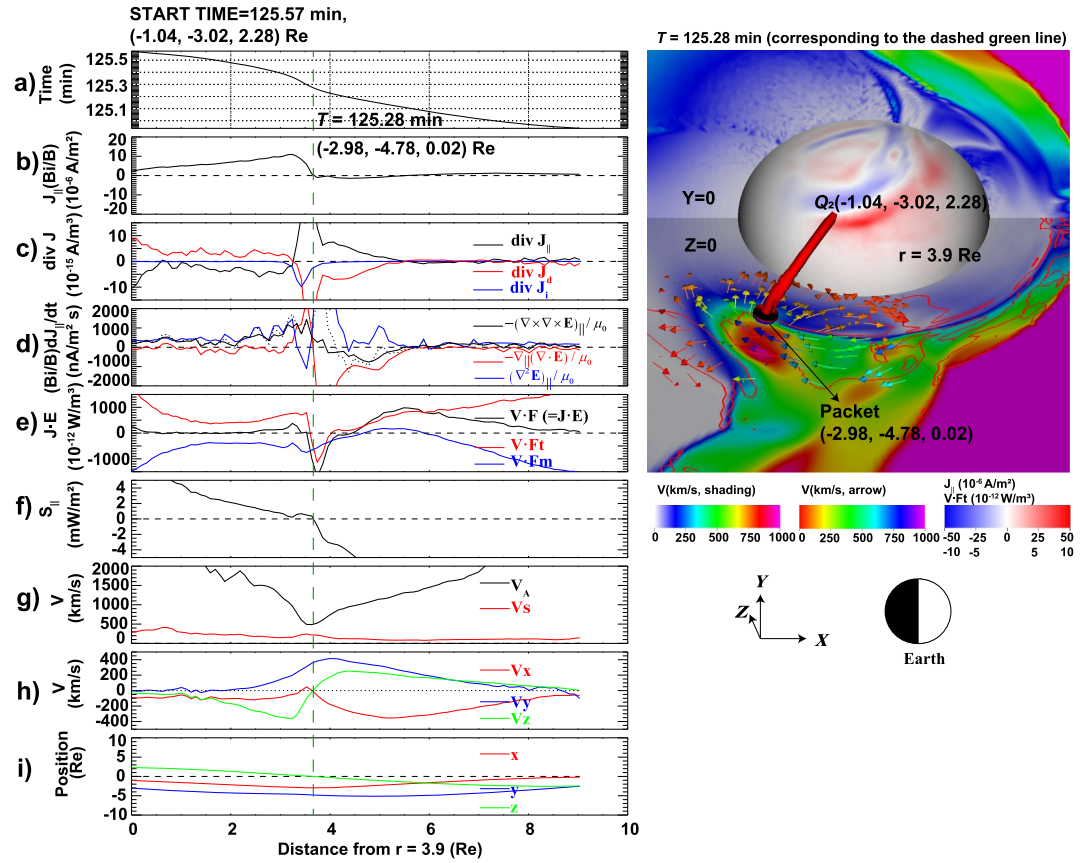


Figure 4. Same as Figure 3 except for the trajectory of the packet of the Alfvén wave associated with MI. The trace started backward in time from point Q_2 at $T = 125.57$ min, and the snapshot is taken at $T = 125.28$ min.

3.3. Generation of FACs

Figure 3 summarized the associated quantities (panels on the left-hand side) taken along the trajectory indicated by a long thin tube in the snapshot on the right, and the location of Alfvén wave packet at $T = 124.3$ min (indicated by the green vertical dashed lines in the left panels) is depicted using a short thick tube in this trajectory. The packet arrived at P_1 (7 MLT, 70 MLAT) in the ionosphere at 124.55 min, where the upward FAC ($J_{\parallel} < 0$, PI-associated FAC on the dawnside) has just begun to develop in the ionosphere. The snapshot on the right column indicates the flow velocity of plasma in the x - y and x - z planes, the FACs on the sphere, with a radius of $3.9 R_E$ and the red contour lines that are plotted to indicate $\mathbf{V} \cdot \mathbf{F}_t = 0$ in the 2 planes. A small plane shows the magnitude of the flow velocity in the x - y plane at $z = 2.7 R_E$ at which the packet intersects at this moment. The color of the tubes (short and long one) indicates $\mathbf{V} \cdot \mathbf{F}_t$. We traced the packet backward in time from the point Q_1 ($0.63, -2.59, 2.84$) R_E on the $3.9 R_E$ sphere, which is mapped to the point P_1 (7 MLT, 70 MLAT) in the ionosphere along the dipole magnetic field line (see Table 1). It is found from Figures 3c–3e that the FACs are generated in the limited region around the green vertical line, where all the criteria mentioned in Section 2.3 are met, that is, $\nabla \cdot \mathbf{J}_{\parallel} < 0$, $\partial J_{\parallel} / \partial t < 0$, and $\mathbf{V} \cdot \mathbf{F}_t < 0$. The generation region is located at off-equator, and for this particular packet, it is located at $(1.2, -5.6, 2.7) R_E$ at $T = 124.3$ min. This belongs to FAC dynamo 1. According to Figure 3c, the FAC is almost closed with the diamagnetic current (\mathbf{J}_d). According to Equation 4, the time rate of change in FACs ($\partial J_{\parallel} / \partial t$) is decomposed into $-\nabla_{\parallel}(\nabla \cdot \mathbf{E}) / \mu_0$ and $(\nabla^2 \mathbf{E})_{\parallel} / \mu_0$. The two terms are indicated by the red and blue lines, respectively in Figure 3d. In this case, they both contribute to the generation of this upward (negative) FAC at the compressional front. Figure 3f shows the parallel component of the Poynting flux defined by

$$S_{\parallel} = \frac{\mathbf{E} \times \mathbf{B}}{\mu_0} \cdot \frac{\mathbf{B}_0}{B_0}, \quad (9)$$

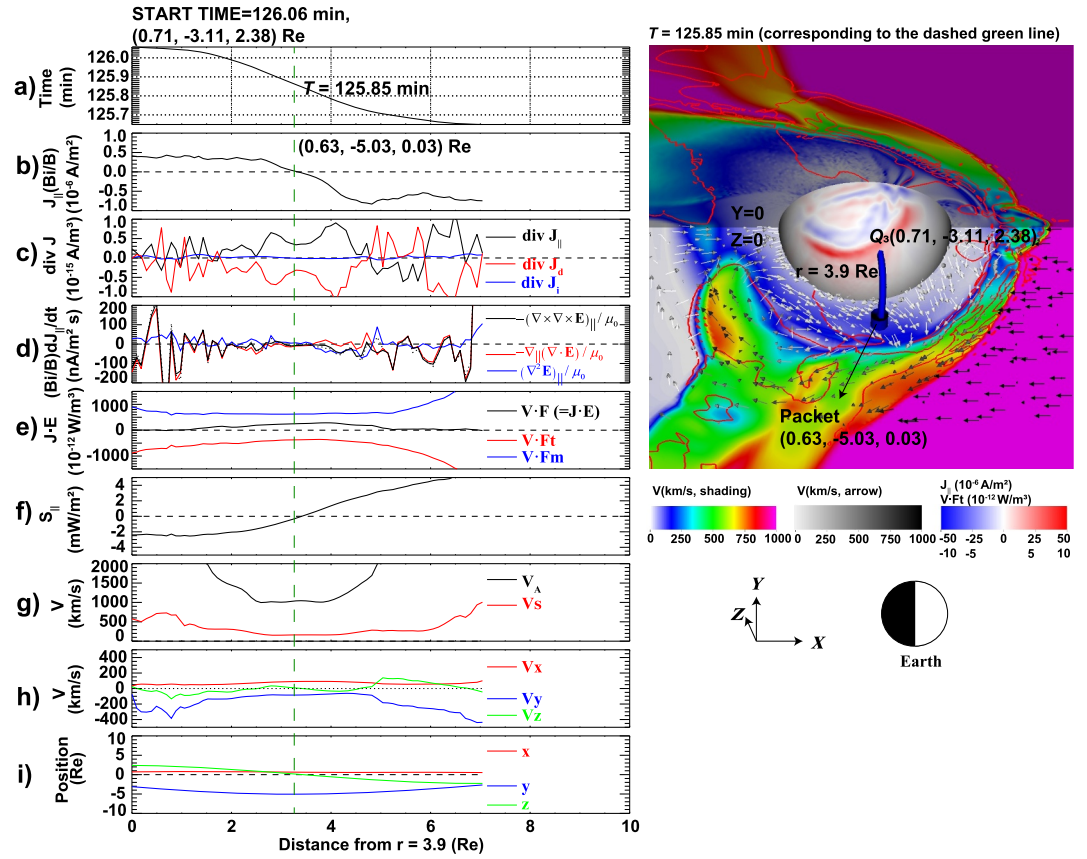


Figure 5. Same as Figure 3 except for the trace starting from point Q_3 at $T = 126.06$ min, and the snapshot taken at $T = 125.85$ min.

where \mathbf{B}_0 is the dipole magnetic field (Ebihara et al., 2020). At the low altitudes where the dipole magnetic field dominates, S_{\parallel} is expected to reasonably represent the Poynting flux associated with the Alfvén waves. Obviously, S_{\parallel} is positive at distance less than $3 R_E$, which indicates that the magnetic energy flows in the direction to the Northern ionosphere out of the region where the FAC is generated. The Alfvén speed V_A shown in Figure 3g increases quickly in a short time, and the plasma is accelerated in the anti-sunward direction at the compressional wave front as shown in Figure 3h. Figure 3i indicates the location of the packet, showing that the generation region for this case is off the equator. The generation mechanism will be discussed in next subsection.

Figure 4 is the same as Figure 3 except for the packet that reached P_2 (5 MLT, 67 MLAT) at 125.57 min, where the downward FAC ($J_{\parallel} > 0$, MI-associated FAC on the dawnside) has begun to develop in the ionosphere. In this case, the three criteria, $\nabla \cdot \mathbf{J}_{\parallel} > 0$, $\partial J_{\parallel} / \partial t > 0$, and $\mathbf{V} \cdot \mathbf{F}_t < 0$, are satisfied around $T = 125.28$ min as shown in Figures 4c–4e. The generation region for the downward FAC is in the vicinity of the equatorial plane, which belongs to FAC dynamo 2. For this specific packet, it crossed the equatorial plane at $(-3.0, -4.8, 0.0) R_E$. According to Figure 4c, the divergence of inertia current (\mathbf{J}_i) plays a minor role in the closure of the FAC compared to the divergence of diamagnetic current (\mathbf{J}_d). In Figure 4d, the two terms $-\nabla_{\parallel}(\nabla \cdot \mathbf{E}) / \mu_0$ (red line) and $(\nabla^2 \mathbf{E})_{\parallel} / \mu_0$ (blue line) both contribute to the time rate of change in FACs ($\partial J_{\parallel} / \partial t$) as well. In contrast to that for FAC dynamo 1, the former term becomes very positive, which results in the increase of the downward FAC. Figure 4e shows $\mathbf{J} \cdot \mathbf{E}$, $\mathbf{V} \cdot \mathbf{F}_t$, and $\mathbf{V} \cdot \mathbf{F}_m$. Though the process of work being performed is much shorter than that for FAC dynamo 1 (see Figure 3e), the effect on the Alfvén wave is larger due to the large amplitude of the rate of the energy conversion. The parallel component of the Poynting flux S_{\parallel} is positive as shown in Figure 4f, implying that the magnetic energy propagates toward the Northern ionosphere from the equatorial plane. When comparing Figures 3h and 4h, it is found that the acceleration of the plasma V_x at the wave front ceases and then decelerates when a flow shear is formed at $x = -3$ and $y = -5 R_E$ near dawn. While the sunward motion is still too slow at this

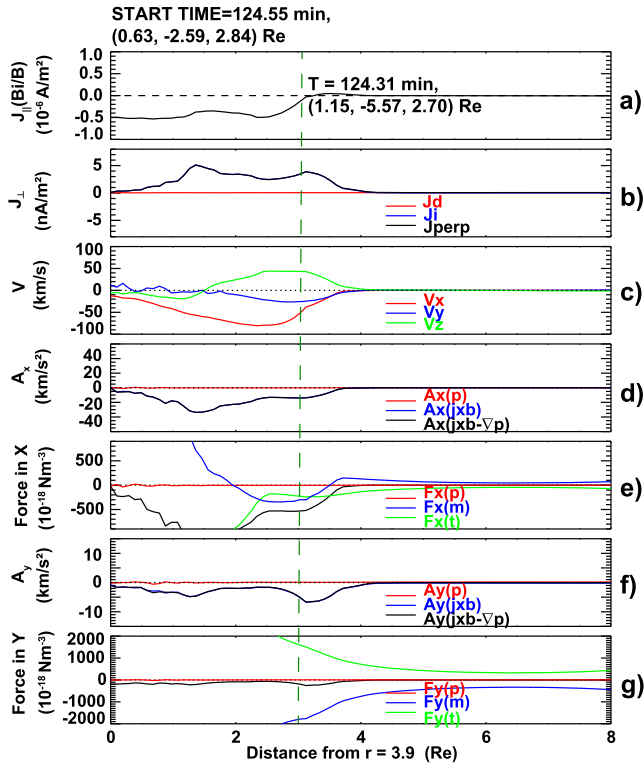


Figure 6. Quantities taken along the trajectory of the packet of the Alfvén wave associated with PI. The horizontal axis marks the distance from $r = 3.9 R_E$. The vertically aligned panels indicate (a) normalized field-aligned current (FAC) $(B_i/B) J_{\parallel}$ (positive parallel and negative anti-parallel to the magnetic field), (b) magnitude of perpendicular currents, including the diamagnetic current J_d and the inertial current J_i , (c) velocity \mathbf{V} , (d) x -component of the acceleration A_x , (e) x -component of the force, where \mathbf{F}_p , \mathbf{F}_t and \mathbf{F}_m are the plasma pressure force, the magnetic tension force and the magnetic pressure force, respectively, (f) y -component of the acceleration A_y , (g) y -component of the force. These quantities are taken along the packet that arrived at P_1 at 124.55 min, at which the upward FAC ($J_{\parallel} < 0$, PI-associated FAC on the dawnside) flows.

indicates that the perpendicular current is dominated by the inertia current, which is also suggested by Fujita and Tanaka (2022). The physical process here is supposed to be as follows. The plasma in front of the compressional wave is accelerated by the Lorentz force, especially the magnetic pressure force. The field line is bent due to frozen-in theorem. The magnetic tension appears in the field line. The plasma performs negative work against the tension force because \mathbf{V} (accelerated by \mathbf{F}_m) is opposite to the tension force (\mathbf{F}_t) and then Alfvén waves are generated.

Figure 7 summarizes the relevant quantities for the case of the generation of downward FACs (MI-associated FACs on the dawnside), corresponding to Figure 4. A large amount of the FACs are connected with the diamagnetic current as shown in Figure 4c, but the magnitude of the diamagnetic current is smaller than that of the inertial current as shown in Figure 7b, which may imply that the magnitude of the currents (the inertial current J_d and the diamagnetic current J_i) does not immediately mean the degree of connection of the FAC. The acceleration is mostly in $+x$ direction because of the strong magnetic tension force as indicated in Figures 7d and 7f. The magnitude of F_t is increasing with the curvature of \mathbf{B} field lines. In this case, the plasma behind the wave front in the equatorial plane is greatly decelerated due to the enhanced tension force.

3.5. Polarity of FACs

It is noticed that the FACs have opposite flowing directions not only during PI and MI phases, but also on the dawnside and duskside. The immediate question is what determines the polarity of the FACs. The polarization of

moment to present a clear vortex structure as shown in Figure 1 by Samsonov & Sibeck (2013). The flow shear is accompanied with the strong downward FAC region.

Figure 5 is the same as Figure 3 except for the packet that reached P_3 (7 MLT, 67 MLAT) at 126.06 min, where the downward FAC ($J_{\parallel} > 0$, MI-associated FAC on the dawnside) is in a fairly steady condition. The third region (where $\mathbf{V} \cdot \mathbf{F}_t < 0$) is present after the passage of the pressure pulse. Although the amplitude is small, the downward FAC persists in the Northern Hemisphere (Figure 5b). $\nabla \cdot \mathbf{J}_{\parallel}$ is, in general, positive (Figure 5c), but $\partial J_{\parallel} / \partial t$ is almost zero (Figure 5d). $\mathbf{V} \cdot \mathbf{F}_t$ is negative all the way along the trajectory of the Alfvén wave packet (Figure 5e). This is also clearly demonstrated in the right panel of Figure 5, that is, the packet that we traced is located in the structure with $\mathbf{V} \cdot \mathbf{F}_t < 0$ (region 3). This structure is expanding from the magnetospheric boundary shown in Figure 1e. Figure 5e shows that S_{\parallel} is negative at distance less than $3.3 R_E$, which means that the magnetic energy flows in the direction anti-parallel to the \mathbf{B} field. The FAC may be generated in the ionosphere and flows into the magnetosphere. It is thus speculated, on the basis of careful diagnosis, that there is no generation of Alfvén waves and the FACs in this region in the magnetosphere. We will discuss the FAC dynamo 1 and two in the following section.

3.4. Mechanism of Generation

In Figures 3 and 4, the generation of upward and downward FACs are identified, which corresponds to FAC dynamo 1 and 2, respectively. The former one is associated with PI, and the latter one is associated with MI, both on the dawnside. The associated generation mechanism is interpreted based on the results shown in Figures 6 and 7 for upward and downward FACs separately. For Figure 6, as to the upward FAC (Figure 6a), it is found that the acceleration of plasma ($\mathbf{A} = (\mathbf{J} \times \mathbf{B} - \nabla P) / \rho$, where P is plasma pressure and ρ is mass density) in the x -direction A_x and in the y -direction A_y (Figures 6d and 6f) is dominated by the Lorentz force ($\mathbf{J} \times \mathbf{B}$). The Lorentz force consists of the magnetic pressure force (\mathbf{F}_m) and the magnetic tension force (\mathbf{F}_t) as shown in Figures 6e and 6g. The former term contributes to the acceleration a little more than the latter. The plasma pressure force ($\mathbf{F}_p = -\nabla P$) almost has no effect on the acceleration of plasma during the generation of upward FACs. Figure 6b

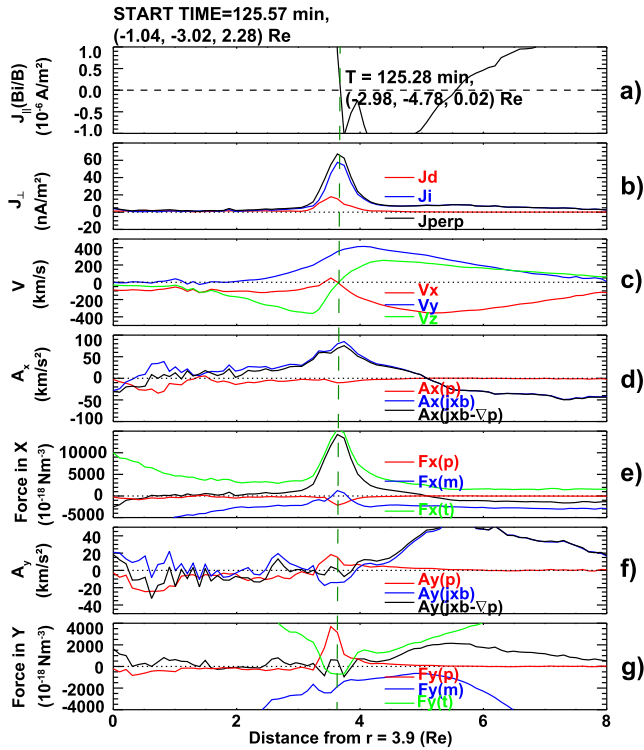


Figure 7. Same as Figure 6 except for the trajectory of the packet of the Alfvén wave associated with MI. These quantities are taken along the packet that arrived at P_2 at 125.57 min, at which the downward field-aligned current (FAC) ($J_{\parallel} > 0$, MI-associated FAC on the dawnside) flows.

the FAC is determined by Equation 4. The second term on the right-hand side of Equation 10 are negative in the generation regions of PI and MI as shown in Figures 3 and 4. That is, the first term on the right-hand side of Equation 4, $-\nabla_{\parallel}(\nabla \cdot \mathbf{E})/\mu_0$, could determine the polarity of the FAC.

According to Equation 4 and the ideal MHD assumption ($\mathbf{E} = -\mathbf{V} \times \mathbf{B}$), we have (when only \mathbf{E}_{\perp} is present)

$$\begin{aligned} \nabla \cdot \mathbf{E}_{\perp} &= \nabla \cdot (-\mathbf{V}_{\perp} \times \mathbf{B}) \\ &= -\mathbf{B} \cdot (\nabla \times \mathbf{V}_{\perp}) + \mathbf{V}_{\perp} \cdot (\nabla \times \mathbf{B}) \\ &= -\mathbf{B} \cdot \boldsymbol{\Omega}_{\parallel} + \mu_0 \mathbf{V}_{\perp} \cdot \mathbf{J}. \end{aligned} \quad (10)$$

where the vorticity is defined as $\boldsymbol{\Omega}_{\parallel} \equiv \nabla \times \mathbf{V}_{\perp}$. Taking the divergence of both sides, we have

$$-\nabla_{\parallel}(\nabla \cdot \mathbf{E}_{\perp}) = \nabla_{\parallel}(\mathbf{B} \cdot \boldsymbol{\Omega}_{\parallel}) - \mu_0 \nabla_{\parallel}(\mathbf{V}_{\perp} \cdot \mathbf{J}). \quad (11)$$

Equation 11 indicates that the term $-\nabla_{\parallel}(\nabla \cdot \mathbf{E})/\mu_0$ consists of two terms. One is associated with the gradient of $(\mathbf{B} \cdot \boldsymbol{\Omega}_{\parallel})$ in the parallel direction, and the other one is associated with the gradient of the dot product of the velocity and the current density in the parallel direction. The gradient in the parallel direction ∇_{\parallel} is calculated based on the localized magnetic field. Since the packet of the Alfvén wave does not move along the magnetic field line, we traced the magnetic field lines starting from the locations of packets in Figure 3 (1.15, $-5.57, 2.70$) R_E and Figure 4 ($-2.98, -4.78, 0.02$) R_E , separately. These points correspond to the generation regions of the PI and MI FACs, respectively.

Figure 8 shows the quantities along the magnetic field line from the generation regions of PI and MI FACs. In the vicinity of the generation region (starting from the leftmost where the tracing distance is zero), three criteria are met as shown in Figures 8b–8d. As discussed previously in Section 3.3, the polarity of the time derivative of FACs is determined by the gradient of $-\nabla_{\parallel}(\nabla \cdot \mathbf{E})$ as indicated in Figure 8e. Figure 8f shows that $(\nabla \times \mathbf{V})_{\parallel}$ with an opposite sense of $(\nabla \cdot \mathbf{E})$ is increasing/decreasing for PI/MI case. According to Equation 11, $-\nabla_{\parallel}(\nabla \cdot \mathbf{E})$ also consists of two components, $\nabla_{\parallel}(\mathbf{B} \cdot \boldsymbol{\Omega}_{\parallel})$ and $\nabla_{\parallel}(\mathbf{V}_{\perp} \cdot \mathbf{J})$. It is found that for PI FAC, the contribution from $\nabla_{\parallel}(\mathbf{B} \cdot \boldsymbol{\Omega}_{\parallel})$ is dominant, and that for MI FAC, the contribution from $\nabla_{\parallel}(\mathbf{V}_{\perp} \cdot \mathbf{J})$ plays an important role. The features of terms $(\nabla \times \mathbf{V})_{\parallel}$ and $(\mathbf{V}_{\perp} \cdot \mathbf{J})$ will be explained in detail later.

Figure 9 shows the magnetic pressure in the equatorial plane and $(\nabla \times \mathbf{V})_{\parallel}$ in the x - y plane at $z = 0$ and $z = 2.7 R_E$. At $T = 123.64$ min before the generation of PI FACs, the compressional wave that is characterized by high magnetic pressure is shown in Figure 9a. Both the distributions of $(\nabla \times \mathbf{V})_{\parallel}$ at $z = 0$ and $z = 2.7 R_E$ are similar at the early stage ($T = 123.64$ min). At this moment, the disturbances associated with the compressional wave have not reached the ionosphere, and FACs in the ionosphere remain low. About half a minute later ($T = 124.23$ min), the distribution of the magnetic pressure is largely changed by the propagation of the compressional wave as shown in Figure 9b. Together with the Earth's intrinsic magnetic field, the gradient of the magnetic pressure gives rise to the varied distribution of $(\nabla \times \mathbf{V})_{\parallel}$ according to the two right panels in Figure 9b. This bump of the high-magnetic pressure region near the equatorial plane coincides with the distribution of $(\nabla \times \mathbf{V})_{\parallel}$ in the equatorial plane. At low z -values ($z = 0$), on the dawnside, the opposite vorticity appears earthward (negative) and anti-earthward (positive) of the protruding high magnetic pressure region in the equatorial plane. At high z -values ($z = 2.7 R_E$), $(\nabla \times \mathbf{V})_{\parallel} > 0$ is still dominant at the wave front because there is no such protrusion. The positive vorticity decreases along the field line, which causes the generation of the upward FAC as shown in Figure 8.

For MI FACs, the contribution from $\nabla_{\parallel}(\mathbf{V}_{\perp} \cdot \mathbf{J})$ is dominant. Figure 10 shows the current density \mathbf{J} and plasma flow velocity \mathbf{V} in the equatorial plane at the moment of MI FAC generation ($T = 125.28$ min). Near the

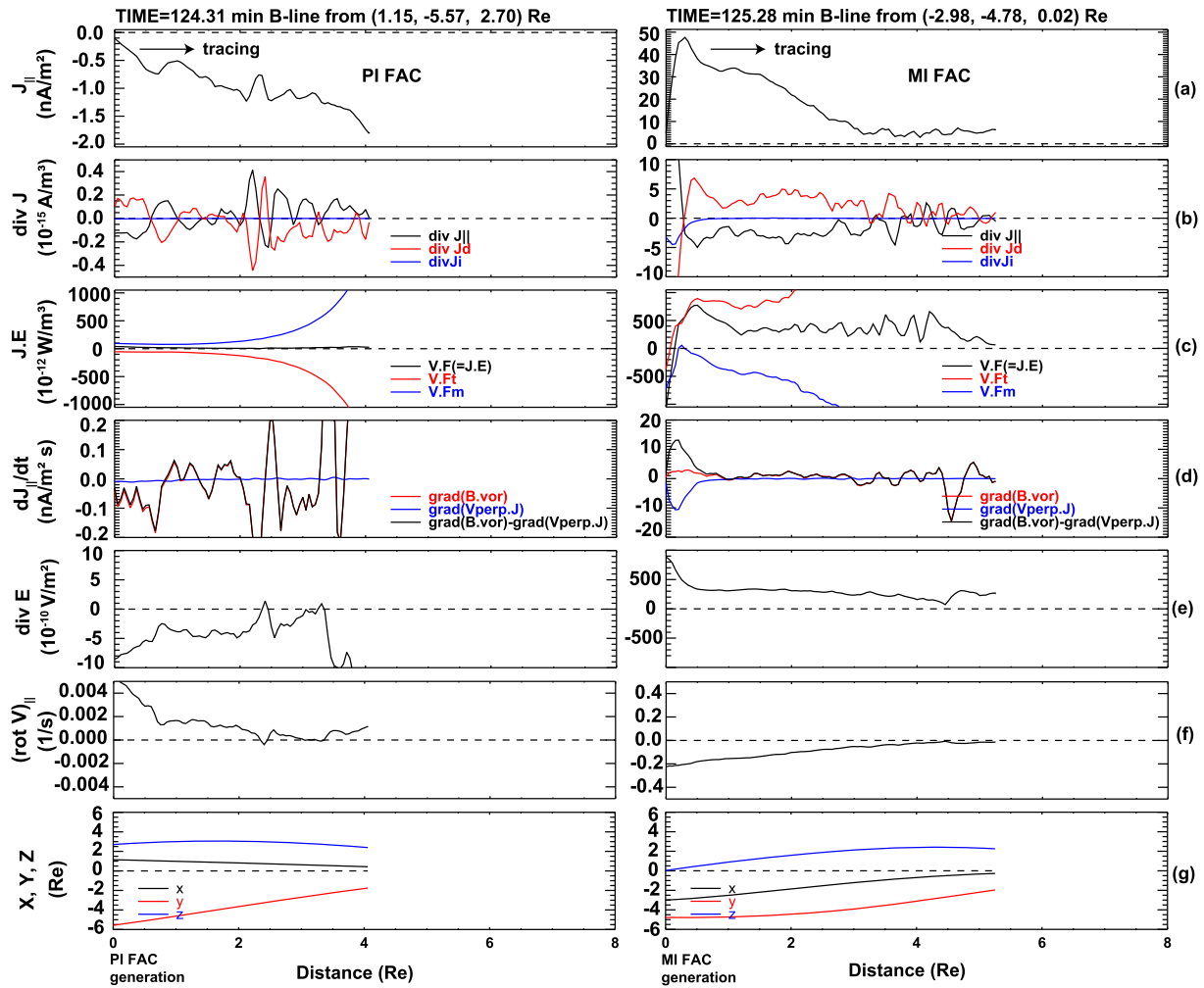


Figure 8. Quantities taken along the field line extending from the packets of Alfvén wave associated with PI (left) and MI (right) field-aligned current (FAC) generation. (a) FAC J_{\parallel} (positive parallel and negative anti-parallel to the magnetic field), (b) $\nabla \cdot \mathbf{J}_{\parallel}$, $\nabla \cdot \mathbf{J}_d$, and $\nabla \cdot \mathbf{J}_i$, where \mathbf{J}_{\parallel} , \mathbf{J}_d and \mathbf{J}_i are the FAC, the diamagnetic current and the inertial current, respectively, (c) $\mathbf{J} \cdot \mathbf{E}$ (black), $\mathbf{V} \cdot \mathbf{F}_t$ (red) and $\mathbf{V} \cdot \mathbf{F}_m$ (blue), where \mathbf{F}_t and \mathbf{F}_m are the magnetic tension force and the magnetic pressure force, respectively, (d) time rate of change in the FAC, $-\nabla_{\parallel}(\nabla \cdot \mathbf{E}_{\perp})$, consists of $\nabla_{\parallel}(\mathbf{B} \cdot \boldsymbol{\Omega}_{\parallel})$ (red line) and $\nabla_{\parallel}(\mathbf{V}_{\perp} \cdot \mathbf{J})$ (blue line), (e) $\nabla \cdot \mathbf{E}$, (f) parallel vorticity $(\nabla \times \mathbf{V})_{\parallel}$, and (g) position $(x, y, z) R_E$.

generation region $(-3.0, -4.8, 0) R_E$, it is found the current (black arrows) is flowing westward on both dawn and dusk sides. The plasma flow (white arrows) is westward on the dawnside, and eastward on the duskside, which causes the dawn-dusk asymmetry in the result of the dot product.

4. Discussions and Summary

We identified the FAC dynamos associated with the SC by tracing Alfvén wave packets. According to the simulation results above, the PI FACs are generated in FAC dynamo 1 that is at the wavefront and off the equator due to the acceleration by the magnetic pressure force, and MI FACs are generated in the equatorial plane where FAC dynamo 2 is located due to the enhanced magnetic tension force that decelerates the plasma. The shape of wavefront in the magnetosphere is not a plane as indicated by Samsonov & Sibeck (2013), and the non-uniformity at different z -values (distance from the equatorial plane) leads to the different distribution of $(\nabla \times \mathbf{V})_{\parallel}$ through the Lorentz force (including both magnetic pressure force and tension force) that determines the polarity of PI FACs. MI FACs are downward/upward on the dawnside/duskside due to the great contribution from $\nabla_{\parallel}(\mathbf{V}_{\perp} \cdot \mathbf{J})$ in the equatorial plane, which may be associated with the rapid enhancement of perpendicular currents in the generation region.

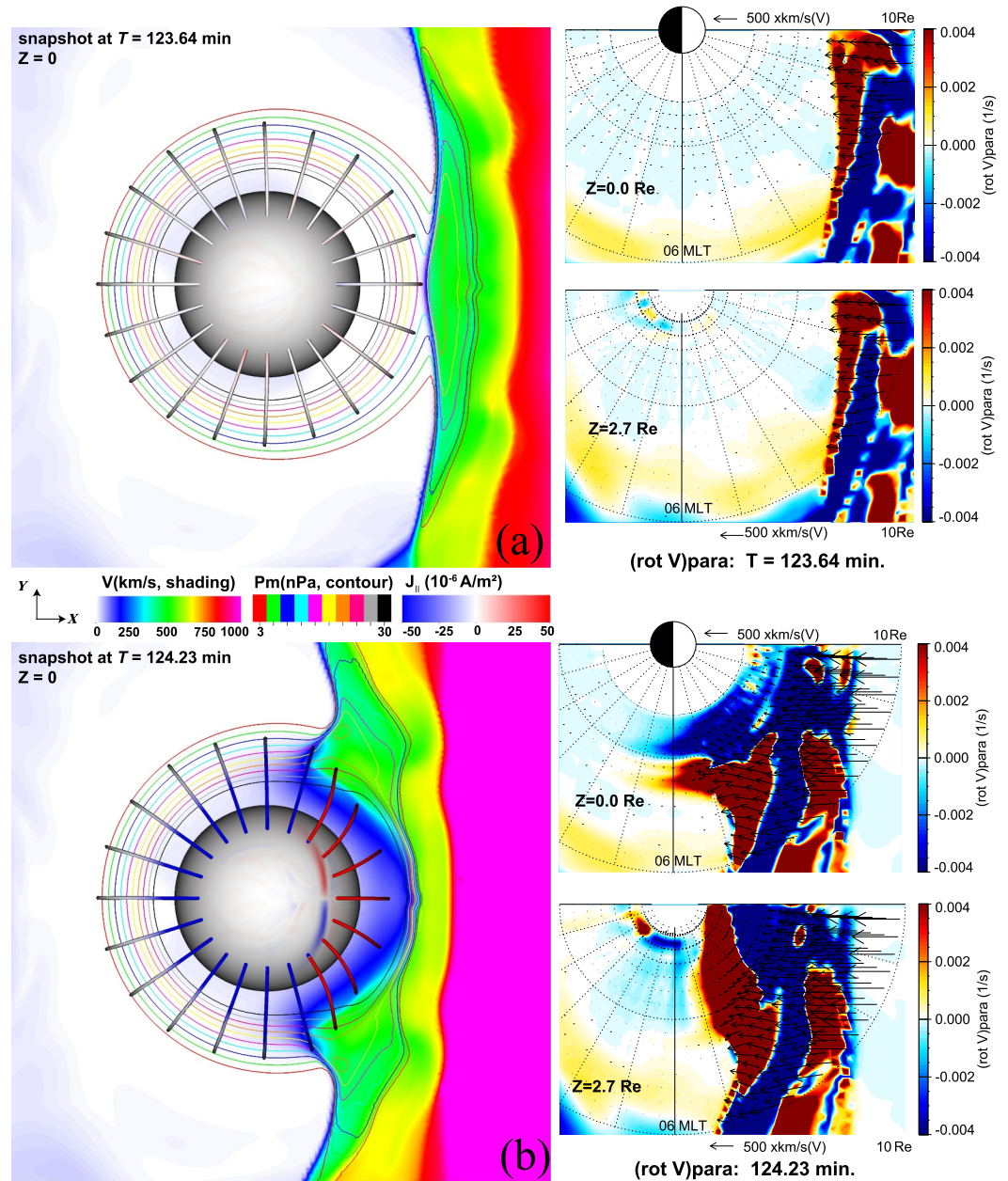


Figure 9. A view from the magnetic north pole. The magnetic pressure structure (contour lines), plasma velocity (color shadings), and field lines are shown in the left column. The distribution of $(\nabla \times \mathbf{V})_{\parallel}$ at different $z = 0$ and $z = 2.7 R_E$ (2 panels on the right). The Sun is to the right. Sub-figure (a) is taken at $T = 123.64$ min; (b) at 124.23 min.

The generation region was identified by condition $\mathbf{J} \cdot \mathbf{E} < 0$ in many previous studies (e.g., Fujita, Tanaka, Kikuchi, Fujimoto, Hosokawa, & Itonaga, 2003; Fujita, Tanaka, Kikuchi, Fujimoto, & Itonaga, 2003; Samsonov et al., 2010). By tracing the current lines, Fujita, Tanaka, Kikuchi, Fujimoto, Hosokawa, and Itonaga (2003) indicated that the PI-associated current is generated in the magnetopause where $\mathbf{J} \cdot \mathbf{E}$ is negative. They point out that at the wavefront region, electromagnetic forces push the plasma, which makes $\mathbf{J} \cdot \mathbf{E}$ become positive. Similarly, Samsonov et al. (2010) found that the plasma is accelerated in the region near the magnetopause where $\mathbf{J} \cdot \mathbf{E} > 0$, and they attributed the dynamo region to the reconfiguration of the magnetic field near the magnetopause. As shown in Figure 3e, $\mathbf{J} \cdot \mathbf{E}$ is indeed positive because the magnitude of $\mathbf{V} \cdot \mathbf{F}_m$ (which is positive) is larger than that of $\mathbf{V} \cdot \mathbf{F}_i$ (which is negative). The plasma is then accelerated by the magnetic pressure force at the

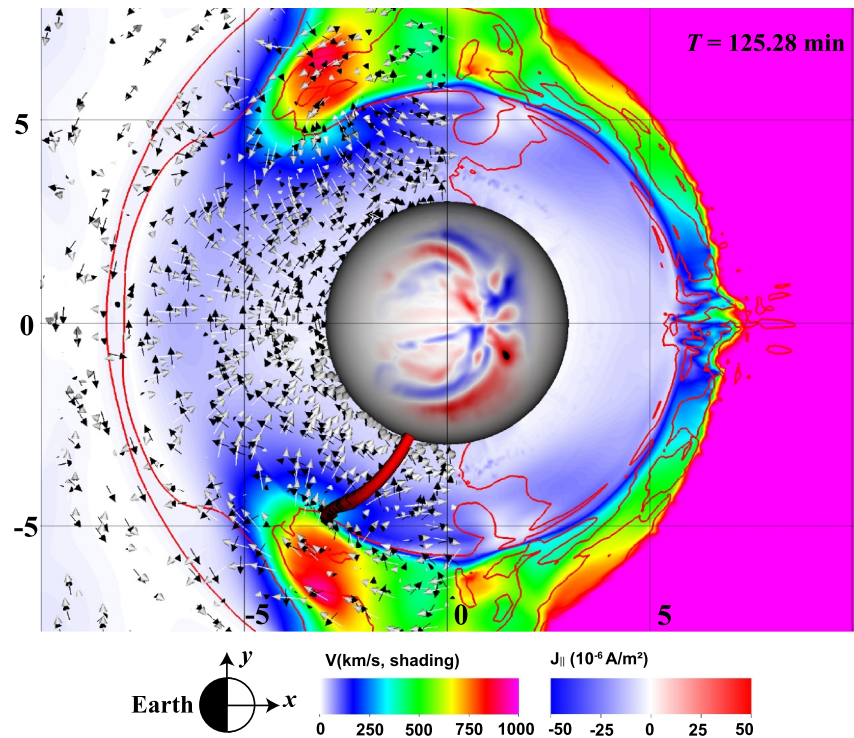


Figure 10. A view from the magnetic north pole at $T = 125.28$ min. MI FAC is generated where the reddish thick tube (the trajectory of packet) crosses the x - y plane. The Sun is to the right. Color bars show the plasma flow velocity in the equatorial plane and the intensity of J_{\parallel} mapped to the sphere $3 R_E$. Red curves indicate where $\mathbf{V} \cdot \mathbf{F}_t = 0$. White and black arrows represent the direction of plasma flow and current in the equatorial plane, separately.

wavefront. The motion of the accelerated plasma gives rise to the bend of magnetic field lines due to the frozen-in theorem, which explains the reason why $\mathbf{V} \cdot \mathbf{F}_t$ is negative and PI FAC is generated as identified in Section 3.3. Thus, the term of $\mathbf{J} \cdot \mathbf{E}$ indicates the energy conversion though, it does not suggest the generation of FACs when the effect from the magnetic pressure force is present.

The generation of FACs associated with the pressure pulse is explained in terms of the PI and MI phases separately in previous studies. Fujita, Tanaka, Kikuchi, Fujimoto, Hosokawa, and Itonaga (2003) suggested that the PI current is converted from an enhanced magnetopause current along the compressional wavefront due to the nonuniformed plasma. The mode conversion takes place in the region where there is a steep gradient of V_A . Their conclusion that the current in the wavefront region is an inertia current, is similar with the dominance of the inertial current in the dynamo region in our simulation as illustrated in Figures 6b and 7b. According to the divergence of the currents shown in Figures 3c, 4a, and 4c large amount of the FACs is connected with the diamagnetic current. Currently, we do not know the reason why FACs are mostly connected to the diamagnetic current, not the inertial current. Fujita and Tanaka (2022) discussed the components of the divergence of the inertia current and the possible mechanisms on the basis of tracing the current lines. This method may result in the different conclusion with that using the method of tracing an Alfvén wave packet (Ebihara & Tanaka, 2024).

The generation mechanism of MI FACs was interpreted as an isolated enhancement of plasma pressure in the equatorial plane, caused by the compression of the magnetospheric flank due to the solar wind impulse, which gives rise to a plasma convection vortex subsequently (Fujita, 2019; Fujita, Tanaka, Kikuchi, Fujimoto, & Itonaga, 2003). In situ observations of magnetospheric vortex on both the dayside and nightside are reported (Shi et al., 2014; Tian et al., 2016 and the references therein). Yu and Ridley (2009) demonstrated that the magnetospheric flow vortex is driven by the plasma pressure gradient. It is found in our simulation that the vortex is moving with a high plasma pressure region in the equatorial plane together with the generation region of the MI FACs (not shown). This plasma flow vortex appears after the sudden compression of the magnetosphere and moves toward the nightside, which is called FAC dynamo 2 as shown in Figure 4. Samsonov & Sibeck, (2013) investigated the large-scale flow vortex following a magnetospheric sudden impulse through global MHD

simulations and suggested that this vortex near the Earth is caused by the interaction between the fast compressional wave and the inner boundary of the simulation model. They claimed that the inner boundary of the simulation model can be regarded as the plasmopause or the ionosphere. Further studies are needed to investigate the overall influence of the inner boundary of the simulation model. In addition, they indicated that the Lorentz force ($\mathbf{J} \times \mathbf{B}$) is involved in the formation of the vortex. The Lorentz force consists of magnetic pressure force (\mathbf{F}_m) and magnetic tension force (\mathbf{F}_t) according to Equation 7. The effect from the former/latter is dominant in the acceleration/deceleration of plasma respectively, which gives rise two different FAC dynamo regions as shown in our result.

The prominent difference between PI and MI FACs is the opposite flowing direction. The PI FAC is flowing out of the ionosphere and the MI FAC is flowing into it on the dawnside. The asymmetry exists not only at different phases (PI and MI), but also on the dawn and dusk side. According to our results, the asymmetry in PI/MI phase is due to the different generation mechanism that the polarity PI FACs is depending on the $\nabla_{\parallel}(\mathbf{B} \cdot \boldsymbol{\Omega}_{\parallel})$, and MI FAC is determined by $\nabla_{\parallel}(\mathbf{V}_{\perp} \cdot \mathbf{J})$. The magnitude of $\boldsymbol{\Omega}_{\parallel} \nabla B$ is much smaller compared to $B \nabla \boldsymbol{\Omega}_{\parallel}$ (not shown) in PI FAC generation region and $\nabla_{\parallel}(\mathbf{V}_{\perp} \cdot \mathbf{J})$ is almost zero in PI case. This implies that polarity of PI FACs is closely related with the field-aligned variation of parallel vorticity $\boldsymbol{\Omega}_{\parallel}$, which also explains the dawn-dusk asymmetry of PI FACs. The dawn-dusk asymmetry of MI FACs is due to the perpendicular current flowing from dawn to dusk (westward) in the equatorial plane, and plasma flow is westward/eastward on dawn/dusk side as shown in Figure 10, which causes the dot product ($\mathbf{V}_{\perp} \cdot \mathbf{J}_{\perp}$) is positive on the dawnside and negative on the duskside. When the strength of MI FACs is enhanced, the gradient will have a different polarity. Many previous studies thought that $\nabla \cdot \mathbf{E}_{\perp}$ is associated with a perpendicular vortex or shear motion ($\boldsymbol{\Omega}_{\perp}$), when $\mathbf{V}_{\perp} \cdot \mathbf{J}_{\perp}$ is omitted (e.g., Araki, 1994; Fujita, Tanaka, Kikuchi, Fujimoto, & Itonaga, 2003; Song & Lysak, 2001; Yu & Ridley, 2009). However, it should be noted that this may be reasonable only for PI case, and the perpendicular current is increasing quickly during MI phase that gives rise to the large field-aligned gradient of $\mathbf{V}_{\perp} \cdot \mathbf{J}_{\perp}$, so it makes the contribution from the term $\nabla_{\parallel}(\mathbf{V}_{\perp} \cdot \mathbf{J})$ nonnegligible and significant as shown in Figure 8d for the MI case.

For the Region 3 in Figure 1, it is found at the very late stage of the MI phase (after 125.14 min) that the negative $\mathbf{V} \cdot \mathbf{F}_t$ region would take over the entire near-Earth space, expanding from near the dayside magnetopause to the magnetotail. This may be explained by the enhanced dawn-to-dusk electric field in the compressed magnetosphere. After the passage of the compressional wavefront toward the nightside, the magnetospheric convection adjusted to the new compressed state of the magnetosphere, since the dynamic pressure of the solar wind remains high due to the continuous high-velocity/density flow in the MHD simulation (Araki, 1994). However, in this case, the time rate of change in FACs is quite minor as shown in Figure 5d, compared to Figures 3d and 4d, even though $\mathbf{V} \cdot \mathbf{F}_t$ is negative all along with the expansion. It is thought that the Alfvén wave packet would have a chance to capture the generation information of FACs several times, or say it is the intersection of different packets in the same region (Ebihara & Tanaka, 2022). Another possibility is that the FAC is generated in the ionosphere, since S_{\parallel} is negative along the trajectory as seen in Figure 5f, indicating that the energy flows from the ionosphere into the magnetosphere. It is thus speculated that there is no generation of FACs in this region in the magnetosphere, given that the three criteria are not all satisfied.

In this study, three criteria are used to identify the generation of the FAC (dynamo) in response to the solar wind dynamic pressure pulse. The generation region and mechanism are interpreted from the perspective of the possible dynamo regions ($\mathbf{V} \cdot \mathbf{F}_t < 0$). The general process of FAC generation associated with the pulse could be summarized as follows.

1. When the solar wind dynamic pressure hits the magnetopause, a compressional wave is excited.
2. As the compressional wave propagates tailward in the magnetosphere, the wavefront forms a protruding part near the equatorial plane. Plasma is accelerated by the magnetic pressure force, and the accelerated plasma pulls the magnetic field line. Alfvén waves are excited, and PI-associated FACs are generated off the equator (FAC dynamo 1).
3. As the compressional wave further propagates, the magnetic field lines are extremely curved, causing the enhancement of magnetic tension force that results in a plasma flow shear. The tension force recovers the bend and gives rise to strong MI-associated FACs due to $\mathbf{V} \cdot \mathbf{F}_t < 0$ (FAC dynamo 2).
4. The polarity of PI FACs is determined by the field-aligned variation of $(\nabla \times \mathbf{V})_{\parallel}$, and polarity of MI FACs is decided by the gradient of $(\mathbf{V}_{\perp} \cdot \mathbf{J})$ in the parallel direction.

Some unsettled issues, like the role of the inner boundary and what determines the connection among FACs, diamagnetic currents and inertial currents, remain for further studies. It is also necessary to investigate in the future the probable instabilities in the magnetosheath and kinetic effects, which may affect the morphology of the compressional front.

Data Availability Statement

The MHD simulation output (run33n.sav) could be found in Zhang et al. (2023a, 2023b) on Zenodo.

Acknowledgments

The computer simulation was performed on the KDK computer system at the Research Institute for Sustainable Humanosphere (RISH), Kyoto University. This study was supported by JSPS KAKENHI Grant 20H01960 and 24K00691, and Mission Research 5–3 and 3 at RISH, Kyoto University.

References

- Akasofu, S.-I., & Chapman, S. (1959). The sudden commencements of geomagnetic storms. *Urania*, 44(250), 321–358.
- Araki, T. (1994). In M. J. Engebretson, K. Takahashi, & M. Scholer (Eds.), *A physical model of the geomagnetic sudden commencement*. American Geophysical Union.
- Araki, T., & Allen, J. H. (1982). Latitudinal reversal of polarization of the geomagnetic sudden commencement. *Journal of Geophysical Research*, 87(A7), 5207–5216. <https://doi.org/10.1029/JA087iA07p05207>
- Cravens, T. E. (1997). *Physics of solar system plasmas*. Cambridge University Press. <https://doi.org/10.1017/CBO9780511529467>
- Ebihara, Y., Lee, L., & Tanaka, T. (2020). Energy flow in the region 2 field-aligned current region under quasi-steady convection. *Journal of Geophysical Research: Space Physics*, 125(2), e2019JA026998. <https://doi.org/10.1029/2019JA026998>
- Ebihara, Y., & Tanaka, T. (2015). Substorm simulation: Insight into the mechanisms of initial brightening. *Journal of Geophysical Research: Space Physics*, 120(9), 7270–7288. <https://doi.org/10.1002/2015JA021516>
- Ebihara, Y., & Tanaka, T. (2022). Where is region 1 field-aligned current generated? *Journal of Geophysical Research: Space Physics*, 127(3), 1–15. <https://doi.org/10.1029/2021JA029991>
- Ebihara, Y., & Tanaka, T. (2023). Generation of field-aligned currents during substorm expansion: An update. *Journal of Geophysical Research: Space Physics*, 128(2), e2022JA031011. <https://doi.org/10.1029/2022JA031011>
- Ebihara, Y., & Tanaka, T. (2024). Generation mechanism of Region 1 field-aligned current and energy transfer from solar wind to polar ionosphere. *Reviews of Modern Plasma Physics*, 8(1), 20. <https://doi.org/10.1007/s41614-024-00154-7>
- Ebihara, Y., Tanaka, T., & Kikuchi, T. (2014). Counter equatorial electrojet and overshielding after substorm onset: Global MHD simulation study. *Journal of Geophysical Research: Space Physics*, 119(9), 7281–7296. <https://doi.org/10.1002/2014JA020065>
- Fujita, S. (2019). Response of the magnetosphere–ionosphere system to sudden changes in solar wind dynamic pressure. *Reviews of Modern Plasma Physics*, 3(1), 2. <https://doi.org/10.1007/s41614-019-0025-1>
- Fujita, S., & Tanaka, T. (2006). Magnetospheric plasma processes during a sudden commencement revealed from a global MHD simulation. *Geophysical Monograph Series*, 31–50. <https://doi.org/10.1029/169GM05>
- Fujita, S., & Tanaka, T. (2022). Two current systems in the preliminary phase of sudden commencements in the magnetosphere. *Earth Planets and Space*, 74(1), 66. <https://doi.org/10.1186/s40623-022-01624-3>
- Fujita, S., Tanaka, T., Kikuchi, T., Fujimoto, K., Hosokawa, K., & Itonaga, M. (2003). A numerical simulation of the geomagnetic sudden commencement: 1. Generation of the field-aligned current associated with the preliminary impulse. *Journal of Geophysical Research*, 108(A12), 1416. <https://doi.org/10.1029/2002JA009407>
- Fujita, S., Tanaka, T., Kikuchi, T., Fujimoto, K., & Itonaga, M. (2003). A numerical simulation of the geomagnetic sudden commencement: 2. Plasma processes in the main impulse. *Journal of Geophysical Research*, 108(A12), 1417. <https://doi.org/10.1029/2002JA009763>
- Fujita, S., Tanaka, T., & Motoba, T. (2005). A numerical simulation of the geomagnetic sudden commencement: 3. A sudden commencement in the magnetosphere–ionosphere compound system. *Journal of Geophysical Research: Space Physics*, 110(A11), 1–8. <https://doi.org/10.1029/2005ja011055>
- Fujita, S., Yamagishi, H., Murata, K. T., Den, M., & Tanaka, T. (2012). A numerical simulation of a negative solar wind impulse: Revisited. *Journal of Geophysical Research*, 117(A9), 1–12. <https://doi.org/10.1029/2012JA017526>
- Guo, X. C., & Hu, Y. Q. (2007). Response of Earth's ionosphere to interplanetary shocks. *Chinese Journal of Geophysics*, 50(4), 817–823. <https://doi.org/10.1002/cjg2.1099>
- Hori, T., Shinbori, A., Nishitani, N., Kikuchi, T., Fujita, S., Nagatsuma, T., et al. (2012). Evolution of negative SI-induced ionospheric flows observed by SuperDARN King Salmon HF radar. *Journal of Geophysical Research*, 117(A12), 1–13. <https://doi.org/10.1029/2012JA018093>
- Iijima, T., & Potemra, T. A. (1976). The amplitude distribution of field-aligned currents at northern high latitudes observed by Triad. *Journal of Geophysical Research*, 81(13), 2165–2174. <https://doi.org/10.1029/JA081i13p02165>
- Itonaga, M., Yoshikawa, A., & Fujita, S. (2000). A wave equation describing the generation of field-aligned current in the magnetosphere. *Earth, Planets and Space*, 52(7), 503–507. <https://doi.org/10.1186/BF03351654>
- Keller, K. A., Hesse, M., Kuznetsova, M., Rastätter, L., Moretto, T., Gombosi, T. I., & Dezeuw, D. L. (2002). Global MHD modeling of the impact of a solar wind pressure change. *Journal of Geophysical Research*, 107(A7), 1–8. <https://doi.org/10.1029/2001JA000060>
- Kikuchi, T., Araki, T., Hashimoto, K. K., Ebihara, Y., Tanaka, T., Nishimura, Y., et al. (2022). Instantaneous achievement of the Hall and Pedersen–Cowling current circuits in northern and southern hemispheres during the geomagnetic sudden commencement on 12 May 2021. *Frontiers in Astronomy and Space Sciences*, 9(May), 1–11. <https://doi.org/10.3389/fspas.2022.879314>
- Kikuchi, T., Hashimoto, K. K., Tomizawa, I., Ebihara, Y., Nishimura, Y., Araki, T., et al. (2016). Response of the incompressible ionosphere to the compression of the magnetosphere during the geomagnetic sudden commencements. *Journal of Geophysical Research: Space Physics*, 121(2), 1536–1556. <https://doi.org/10.1002/2015JA022166>
- Matsushita, S. (1957). On sudden commencements of magnetic storms at higher latitudes. *Journal of Geophysical Research*, 62(1), 162–166. <https://doi.org/10.1029/JZ062i001p0162>
- Moretto, T., Ridley, A. J., Engebretson, M. J., & Rasmussen, O. (2000). High-latitude ionospheric response to a sudden impulse event during northward IMF conditions. *Journal of Geophysical Research*, 105(A2), 2521–2531. <https://doi.org/10.1029/1999JA900475>
- Neubauer, F. M. (1980). Nonlinear standing Alfvén wave current system at IO: Theory. *Journal of Geophysical Research*, 85(A3), 1171–1178. <https://doi.org/10.1029/JA085iA03p01171>
- Samsonov, A. A., & Sibeck, D. G. (2013). Large-scale flow vortices following a magnetospheric sudden impulse. *Journal of Geophysical Research: Space Physics*, 118(6), 3055–3064. <https://doi.org/10.1002/jgra.50329>

- Samsonov, A. A., Sibeck, D. G., & Imber, J. (2007). MHD simulation for the interaction of an interplanetary shock with the Earth's magnetosphere. *Journal of Geophysical Research*, *112*(A12), 1–9. <https://doi.org/10.1029/2007JA012627>
- Samsonov, A. A., Sibeck, D. G., & Yu, Y. (2010). Transient changes in magnetospheric-ionospheric currents caused by the passage of an interplanetary shock: Northward interplanetary magnetic field case. *Journal of Geophysical Research*, *115*(1), 1–12. <https://doi.org/10.1029/2009JA014751>
- Shi, Q. Q., Hartinger, M. D., Angelopoulos, V., Tian, A. M., Fu, S. Y., Zong, Q.-G., et al. (2014). Solar wind pressure pulse-driven magnetospheric vortices and their global consequences. *Journal of Geophysical Research: Space Physics*, *119*(6), 4274–4280. <https://doi.org/10.1002/2013JA019551>
- Sibeck, D. G. (1990). A model for the transient magnetospheric response to sudden solar wind dynamic pressure variations. *Journal of Geophysical Research*, *95*(A4), 3755. <https://doi.org/10.1029/ja095ia04p03755>
- Siscoe, G. L., Crooker, N. U., Erickson, G. M., Sonnerup, B. U. Ö., Siebert, K. D., Weimer, D. R., et al. (2000). Global geometry of magnetospheric currents inferred from MHD simulations. *Geophysical Monograph Series*, 41–52. <https://doi.org/10.1029/GM118p0041>
- Song, Y. A. N., & Lysak, R. L. (2001). Towards a new paradigm: From a quasi-steady description to a dynamical description of the magnetosphere. *Space Science Reviews*, *95*(1/2), 273–292. <https://doi.org/10.1023/A:1005288420253>
- Sun, T. R., Wang, C., Zhang, J. J., Pilipenko, V. A., Wang, Y., & Wang, J. Y. (2014). The chain response of the magnetospheric and ground magnetic field to interplanetary shocks. *Journal of Geophysical Research: Space Physics Abstract*, *120*(1), 157–165. <https://doi.org/10.1002/2014JA020754>
- Tamao, T. (1964). A hydromagnetic interpretation of geomagnetic SSC. *Report of Ionosphere and Space Research in Japan*, *18*, 18–31.
- Tanaka, T. (1994). Finite volume TVD scheme on an unstructured grid system for three-dimensional MHD simulation of inhomogeneous systems including strong background potential fields. *Journal of Computational Physics*, *111*(2), 381–389. <https://doi.org/10.1006/jcph.1994.1071>
- Tanaka, T. (1995). Generation mechanisms for magnetosphere-ionosphere current systems deduced from a three-dimensional MHD simulation of the solar wind-magnetosphere-ionosphere coupling processes. *Journal of Geophysical Research*, *100*(A7), 12057–12074. <https://doi.org/10.1029/95JA00419>
- Tanaka, T. (2015). Substorm auroral dynamics reproduced by advanced global Magnetosphere–Ionosphere (M–I) coupling simulation. In *Auroral dynamics and space weather* (pp. 177–190). <https://doi.org/10.1002/9781118978719.ch13>
- Tian, A. M., Shen, X. C., Shi, Q. Q., Tang, B. B., Nowada, M., Zong, Q. G., et al. (2016). Dayside magnetospheric and ionospheric responses to solar wind pressure increase: Multispacecraft and ground observations. *Journal of Geophysical Research: Space Physics*, *121*(11), 813–830. <https://doi.org/10.1002/2016JA022459>
- Walker, A. D. (2008). Ray tracing of magnetohydrodynamic waves in geospace waves in uniform media. *URSI Radio Science Bulletin*, *325*(325), 24–35. <https://doi.org/10.23919/URSIRSB.2008.7909583>
- Wilson, C. R., & Sugiura, M. (1961). Hydromagnetic interpretation of sudden commencements of magnetic storms. *Journal of Geophysical Research*, *66*(12), 4097–4111. <https://doi.org/10.1029/JZ066i012p04097>
- Wright, A. N., & Southwood, D. J. (1987). Stationary Alfvénic structures. *Journal of Geophysical Research*, *92*(A2), 1167–1175. <https://doi.org/10.1029/JA092iA02p01167>
- Yu, Y., Cao, J., Pu, Z., Jordanova, V. K., & Ridley, A. (2022). Meso-scale electrodynamic coupling of the Earth magnetosphere-ionosphere system. *Space Science Reviews*, *218*(8), 74. <https://doi.org/10.1007/s11214-022-00940-0>
- Yu, Y., & Ridley, A. J. (2009). The response of the magnetosphere-ionosphere system to a sudden dynamic pressure enhancement under southward IMF conditions. *Annales Geophysicae*, *27*(12), 4391–4407. <https://doi.org/10.5194/angeo-27-4391-2009>
- Yu, Y.-Q., & Ridley, A. J. (2011). Understanding the response of the ionosphere-magnetosphere system to sudden solar wind density increases. *Journal of Geophysical Research*, *116*(A4), A04210. <https://doi.org/10.1029/2010JA015871>
- Zhang, T., Ebihara, Y., & Tanaka, T. (2023a). Nighttime geomagnetic response to jumps of solar wind dynamic pressure: A possible cause of québec blackout in march 1989. *Space Weather*, *21*(11), e2023SW003493. <https://doi.org/10.1029/2023SW003493>
- Zhang, T., Ebihara, Y., & Tanaka, T. (2023b). MHD simulation output for jumps of solar wind dynamic pressure (Version 1) [Dataset]. *Zenodo*. <https://doi.org/10.5281/zenodo.7945350>
- Zmuda, A. J., & Armstrong, J. C. (1974). The diurnal flow pattern of field-aligned currents. *Journal of Geophysical Research*, *79*(31), 4611–4619. <https://doi.org/10.1029/JA079i031p04611>